Available online at www.sciencedirect.com
ScienceDirect
Journal of Solid State Chemistry 180 (2007) 296–300
JOURNAL OF SOLID STATE CHEMISTRY
www.elsevier.com/locate/jssc

Cation distribution and magnetic properties in chromium-substituted nickel ferrites prepared using aerosol route

Sonal Singhal[a], Kailash Chandra[b,*]

[a]Department of Chemistry, Panjab University, Chandigarh 160 014, India
[b]Institute Instrumentation Centre, Indian Institute of Technology-Roorkee, Roorkee 247 667, India

Received 6 August 2006; received in revised form 3 October 2006; accepted 9 October 2006
Available online 19 October 2006

Abstract

Cation distribution have been investigated using X-ray diffraction, magnetic and Mössbauer spectral studies in chromium-substituted nickel ferrites prepared by aerosol route. Cation distribution indicates that the chromium atom occupy octahedral site upto $x = 0.8$, and then also enters into tetrahedral site. The saturation magnetization decreases linearly with the increase of chromium concentration due to the diamagnetic nature of the Cr^{3+}. However, interesting behaviour is observed in the coercivity. Initially it increases slowly with the chromium concentration but when $x > 0.8$ a very large increase has been observed. This was attributed to the specific cation distribution of Cr^{3+} which results an unquenched orbital angular momentum and a large anisotropy. Room temperature Mössbauer spectra of as obtained samples exhibited a broad doublet resolved into two doublets corresponding to the surface and internal region atoms. The samples annealed at 1200 °C show broad sextets, which were fitted with different sextets, indicating different local environment of both tetrahedral and octahedral coordinated iron cation.

Keywords: Nano-particles; Saturation magnetization; Coercivity; X-ray diffraction; Mössbauer spectra; Cation distribution

1. Introduction

Nickel ferrite, a typical inverse spinel ferrite, have been extensively used in electronic devices because of their large permeability at high frequency, remarkably high electrical resistivity, mechanical hardness, chemical stability and cost effectiveness [1,2]. Substituted nickel ferrites are widely used as magnetic materials due to their high electrical resistivity, low eddy current and dielectric losses [3,4]. The magnetic properties of materials are strongly affected when the particle size approaches a critical diameter, below which each particle is a single domain. As a result the influence of thermal energy over the magnetic moment ordering leads to super paramagnetic relaxation [5,6].

The effect of substitution of Fe^{3+} by Cr^{3+} in $NiFe_2O_4$ have been studied by various workers [7–9] and showed that Cr^{3+} always seeks to the octahedral sites. Lee et al. [7] studied the chromium-substituted nickel ferrites and reported that Ni^{2+} moves to tetrahedral site within the range $0.2 < x < 0.6$. They showed that the magnetic moment and Curie temperature decreases with the chromium substitution. Fayek and Ata Allah [8] reported that Cr^{3+} content to the octahedral sites for a maximum of $x = 0.6$ and the excess Cr^{3+} replaces the Fe^{3+} at the tetrahedral site. Gismelseed and Yousif [9] studied the Cr^{3+}-substituted $NiCr_xFe_{1-x}O_4$ $(0 < x < 1.4)$ prepared through conventional double sintering ceramic technique and suggested that as the Cr^{3+} substitution increases, the system is slowly converted into a normal spinel structure. Ghatage et al. [10] studied neutron diffraction studies in chromium-substituted nickel ferrite and suggested that the spinels $(x < 0.8)$ have Neel-type magnetic order and for $(x > 0.8)$ the magnetic order is not of the Neel type. Satya et al. [11] reported that the end product of the series, $NiCr_2O_4$ is essentially a normal spinel and a transition occurs from cubic to tetragonal at about 310 K.

The investigations of cation distribution provide a mean to develop materials with desired properties which are

*Corresponding author. Fax: +91 1332 273560.
E-mail addresses: sonal1174@gmail.com (S. Singhal), chandfuc@iitr.ernet.in (K. Chandra).

0022-4596/$ - see front matter © 2006 Elsevier Inc. All rights reserved.
doi:10.1016/j.jssc.2006.10.010

useful in the industry. The present work deals with the cation distribution in chromium-substituted nickel ferrite ($NiCr_xFe_{2-x}O_4$ with $x = 0$, 0.2, 0.4, 0.6, 0.8, 1.0 and 1.2) synthesized via aerosol route. Aerosol technology is the key process for large-scale production of nano-structured materials. Using this method particle size, degree of agglomeration, chemical homogeneity can be controlled easily [12,13]. The cation distribution investigated through XRD, magnetic measurements and Mössbauer spectroscopy.

2. Experimental

Nano-particles of chromium-substituted nickel ferrites were prepared via aerosol route using a setup described in our earlier paper [14,15]. The desired proportions of nickel, chromium and iron nitrates were weighed and dissolved in water to prepare 5×10^{-2} M solutions. Air pressure, sample uptake and furnace temperature were maintained at 40 psi, 3–4 mL/min and ~600 °C, respectively during preparation. The ferrite powder was deposited on the teflon-coated pan.

The elemental analysis was carried out on an electron probe micro-analyzer (EPMA) (JEOL, 8600M) and atomic absorption spectrophotometer (AAS) (GBC, Avanta), while the particle morphology was examined under transmission electron microscope (TEM) (Philips, EM400). The X-ray diffraction (XRD) studies were carried on X-ray spectrometer (Bruker AXS, D8 Advance) with Fe$K\alpha$ radiation and magnetic measurements were made on a vibrating sample magnetometer (VSM) (155, PAR). Mössbauer spectra were recorded on a constant acceleration transducer driven Mössbauer spectrometer using ^{57}Co(Rh) source of 25 mCi initial activity. The spectrometer was calibrated using a natural iron foil.

3. Results and discussion

Elemental analytical confirmed the composition of the ferrites data using EPMA. The TEM micrographs for the as obtained powder showed that the particles of size ~10 nm and the amorphous nature of the sample as described in our earlier papers [14,15]. The micrographs for the annealed sample at various temperatures indicates that the increase of particle size with the annealing temperature [16,17].

The powder X-ray diffractographs were recorded for all the as obtained samples and those annealed at various temperatures. The diffraction pattern of the as obtained samples confirms the amorphous nature of the samples. Peaks become sharp as the annealing temperature increases, which can be attributed to the grain growth at higher temperatures. The crystallite size was calculated from the most intense peak (311) using Sherrer equation [18]. It is seen that the particle size increases from ~16 nm to ~82 nm as the annealing temperatures are raised from 400 to 1200 °C. Fig. 1 represents X-ray powder diffraction

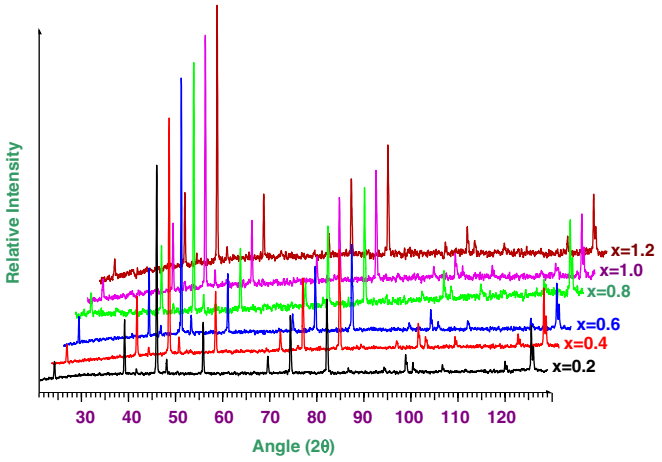

Fig. 1. X-ray diffractographs of the chromium-substituted nickel ferrites ($NiCr_xFe_{2-x}O_4$).

patterns of all the ferrite compositions annealed at 1200 °C. The lattice parameters were calculated using Powley as well as Le Bail refinement methods and are listed in Table 1. All the samples are found to be face centred cubic with Fd-3m space group. It is observed that lattice parameter 'a' decreases linearly with increase in chromium concentration; Fig. 2. This decrease is expected in view of the fact that ionic radius of Cr^{3+} is lower than that of Fe^{3+}. The decrease in 'a' and shift of peak towards higher angle with the increasing chromium concentration; Fig. 1 and 2 shows that Cr^{3+} ions have entered substitutionally incorporated into the spinel structure [19].

In order to determine the distribution of cations over the available tetrahedral (A) and octahedral (B) sites in $NiCr_xFe_{2-x}O_4$ intensities were calculated using the formula suggested by Buerger [20] as

$$I_{hkl} = |F_{hkl}|^2 P L_p,$$

where I_{hkl} is the relative integrated intensity; F_{hkl} the structure factor; P the multiplicity factor; L_p the Lorentz polarization factor $= 1 + \mathrm{Cos}^2 2\theta / \mathrm{Sin}^2 \theta \, \mathrm{Cos}\, \theta$; where θ is the Bragg's angle.

According to Ohnishi and Teranishi [21], the intensity ratios of planes $I_{(220)/I(400)}$, $I_{(400)/I(440)}$ and $I_{(422)/I(400)}$ are considered to be sensitive to the cation distribution. The distribution of Ni^{2+}, Cr^{3+} and Fe^{3+} cations amongst the octahedral and tetrahedral sites in the $NiCr_xFe_{2-x}O_4$ was determined from the X-ray intensity ratio calculations. Calculations of intensity for the planes are made for various possible values of the distribution parameter. The value of the distribution parameter is reached by comparing theoretical and experimental intensity ratio of the above-mentioned planes. The value of distribution parameter for which the theoretical and experimental ratios agree clearly, is taken to be the correct one. The ionic configuration based on the site preference energy value for individual cation suggested that Ni^{2+} ions can occupy only B-sites [22]. Finally the cation distribution is estimated for the best-fit X-ray intensity ratio given in Table 1. This data

Table 1
Lattice parameters and magnetic of the ferrites after annealing at 1200 °C

Ferrite compositions	Lattice parameter a (Å)	Volume (Å^3)	Saturation mag. (emu g^{-1})	Coercivity (G)	n_B (BM)	Cation distributions
$NiFe_2O_4$	8.3365	579.36	47.60	18	2.00	$[Fe_{1.0}]^A[Ni_{1.0}Fe_{1.0}]^B$
$NiCr_{0.2}Fe_{1.8}O_4$	8.3269	577.36	38.40	30	1.61	$[Fe_{1.0}]^A[NiCr_{0.2}Fe_{0.8}]^B$
$NiCr_{0.4}Fe_{1.6}O_4$	8.3188	575.68	26.20	45	1.19	$[Fe_{1.0}]^A[Ni_{1.0}Cr_{0.4}Fe_{0.6}]^B$
$NiCr_{0.6}Fe_{1.4}O_4$	8.3102	573.90	17.70	58	0.77	$[Fe_{1.0}]^A[Ni_{1.0}Cr_{0.6}Fe_{0.4}]^B$
$NiCr_{0.8}Fe_{1.2}O_4$	8.3038	572.57	8.55	90	0.38	$[Fe_{1.0}]^A[NiCr_{0.8}Fe_{0.2}]^B$
$NiCr_{1.0}Fe_{1.0}O_4$	8.2974	571.25	4.82	410	0.20	$[Fe_{0.8}\ Cr_{0.2}]^A[NiCr_{0.8}Fe_{0.2}]^B$
$NiCr_{1.2}Fe_{0.8}O_4$	8.2922	570.18	1.65	2070	0.07	$[Fe_{0.6}Cr_{0.4}]^A[NiCr_{0.8}Fe_{0.2}]^B$

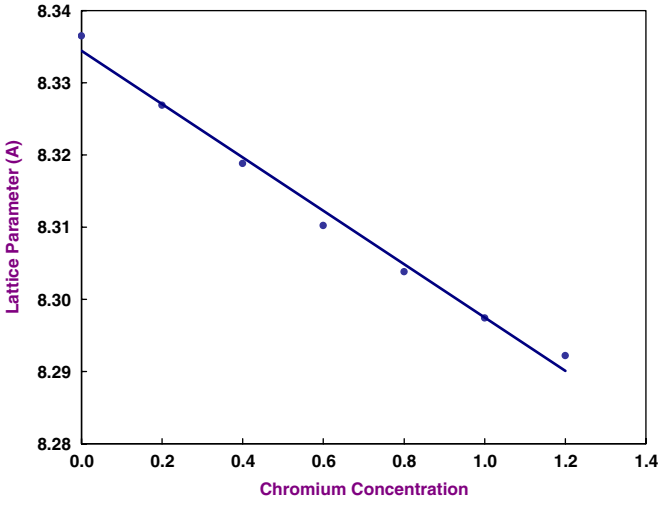

Fig. 2. Variation of lattice parameter with chromium concentration.

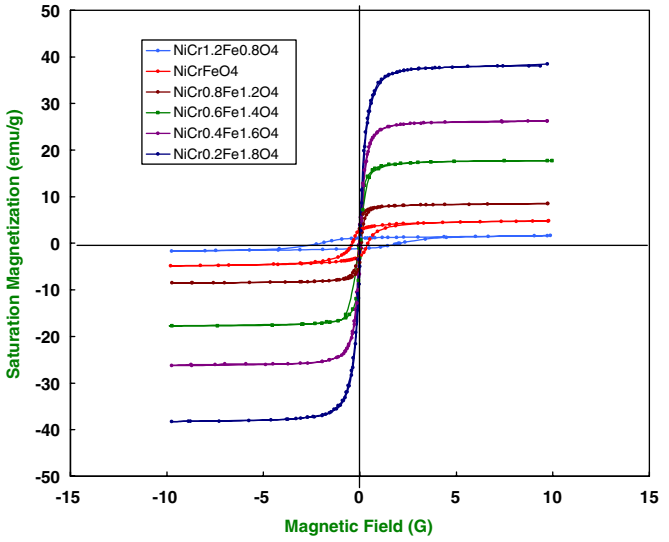

Fig. 3. Hysterisis loop of chromium-substituted nickel ferrites after annealing at 1200 °C.

indicates that the Cr^{3+} ions enters into tetrahedral site when $x = 0.8$ and after that Cr^{3+} occupying both tetrahedral as well as octahedral sites.

Magnetic hysteresis loops, at room temperature were recorded for all the as obtained as well as annealed samples. Typical loops for all the samples annealed at 1200 °C are shown in Fig. 3. The as obtained sample exhibits no hysteresis, which may be attributed to super-paramagnetic relaxation inconformity with the XRD result. The saturation magnetization for all the ferrites after annealing at 1200 °C are listed in Table 1 indicates that M_s decreases with the increase of chromium concentration. This may be attributed to the weakening of exchange interactions due to non-magnetic Cr^{3+} ions. From Table 1 it is clear that the coercivity increases with the chromium concentration slowly up to the concentration $x = 0.8$ after which the coercivity starts increasing steeply (Fig. 4). This behaviour of coercivity may be understood as described by Banerjee and O'Reilly [23] on the basis of a new model for cation distribution. As already discussed in XRD and later on in Mössbauer studies it is confirmed that the chromium ions enters into the tetrahedral site when $x > 0.8$. According to the cation distribution model [23] when Cr^{3+} ions occupy tetrahedral sites it causes a negative trigonal field to be superimposed on the octahedral Cr^{3+} ions. Due to which a two-fold degeneracy of the

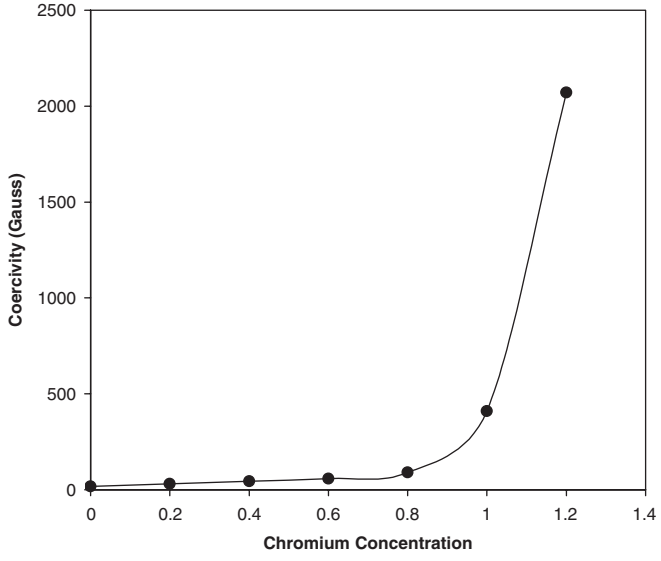

Fig. 4. Variation of the coercivity with chromium concentration.

orbital ground state results in an unquenched orbital angular momentum and a large anisotropy.

Cation distribution calculated using the saturation magnetization per formula unit in Bohr magnetron at

300 K obtained from magnetization data for all the samples are summarized in Table 1. The magnetic moment per formula unit in Bohr magneton (μ_B) was calculated by using the relation:

n_B = M.wt. × Saturation magnetization/5585.

According to the Neel's two sublattices model of ferrimagnetism [24], the magnetic moment per formula unit in μ_B, n_B^N is expressed as

$$n_B^N(x) = M_B(x) - M_A(x),$$

where M_B and M_A are the B and A sublattice magnetic moment in μ_B. The values of Neel's magnetic moment n_B^N were calculated by taking ionic magnetic moment of Fe^{3+}, Cr^{3+} and Ni^{2+} as $5\mu_B$, $3\mu_B$ and $2\mu_B$, respectively. The cation distribution calculated using the magnetic moment data clearly indicates that the Cr^{3+} occupying the octahedral sites upto $x = 0.8$. However, for the composition $x > 0.8$ Neel's theory do not remain valid in conformity with the earlier studies [10].

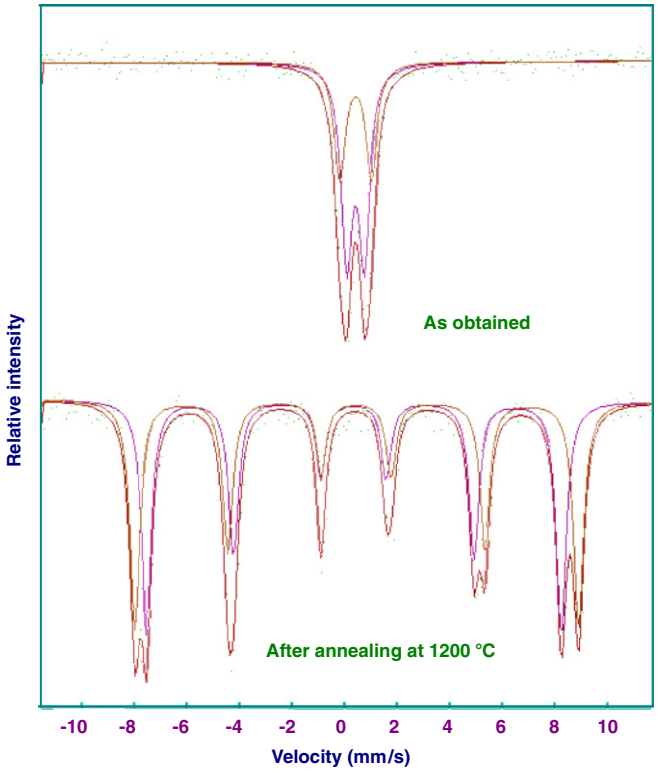

Fig. 5. Mössbauer spectra of $NiFe_2O_4$.

Fig. 5(a) shows the typical Mössbauer spectra of as obtained samples of $NiFe_2O_4$. The presence of broad doublet indicates the superparamagnetic nature of the sample [25]. This broad doublet was fitted with the two sets of the doublets. Since in the small particles (<10 nm) a large fraction of atoms reside on the surface, a different environment is experienced by them as compared to those inside the particle. Therefore, these doublets correspond to the quadrupole splitting of the iron nuclei in the surface region and the internal region of the particles. The Mössbauer data after the least square fitting are given in Table 2. From the data it can be seen that isomer shift for both the doublets are same. However, the quadrupole splitting in the surface region (0.83–1.28 mm s^{-1}) is much larger than the quadrupole splitting in the internal region (0.42–0.74 mm s^{-1}). This can be attributed to the existence of a broader distribution of interatomic spacing and partly disordering in the surface region of the ultrafine particle [26]. It is clear that the contribution of surface region atoms is ~38–42% of the total area of the experiment spectrum. This is in agreement with the percentage (44%) of the volume of the surface region in total volume of the particle with an average grain size (8 nm) by Ma et al. [25]. The quadrupole splitting for both the sites increases linearly with the substitution of Fe^{3+} by Cr^{3+} due to higher electric field asymmetry in the surface region of the particle (Fig. 6) [27].

The Mössbauer spectra recorded at 300 K after annealing at 1200 °C for all the samples exhibit two normal zeeman split sextets due to the A-site Fe^{3+} ions and the other due to B-site Fe^{3+}, which indicates ferrimagnetic behaviour of the samples. A typical Mössbauer spectrum of $NiFe_2O_4$ is given in Fig. 5(b). The variation in the mean hyperfine field acting on A and B sites ^{57}Fe nuclei with chromium concentration are shown in Fig. 7. It is evident

Table 2
Mössbauer parameters of the chromium-substituted nickel ferrites as obtained and after annealing at 1200 °C

Ferrite composition	As obtained					Annealed samples					
	Internal region		Surface region		Surface region (%)	Tetrahedral		Octahedral		FWHM Γ (mm s^{-1})	(%) Intensity of octahedral site
	δ (Fe) (mm s^{-1})	ΔEQ (mm s^{-1})	δ(Fe) (mm s^{-1})	ΔEQ (mm s^{-1})		δ(Fe) (mm s^{-1})	H_{eff} (kOe)	δ(Fe) (mm s^{-1})	H_{eff} (kOe)		
$NiFe_2O_4$	0.45	0.42	0.43	0.83	38.2	0.44	525	0.37	491	0.27	49.8
$NiCr_{0.2}Fe_{1.8}O_4$	0.44	0.45	0.44	0.95	38.6	0.43	513	0.37	485	0.29	43.8
$NiCr_{0.4}Fe_{1.6}O_4$	0.46	0.53	0.45	1.02	37.5	0.42	502	0.39	477	0.28	38.0
$NiCr_{0.6}Fe_{1.4}O_4$	0.46	0.58	0.46	1.09	36.3	0.41	492	0.38	468	0.30	27.5
$NiCr_{0.8}Fe_{1.2}O_4$	0.44	0.65	0.44	1.16	40.5	0.42	479	0.36	456	0.27	17.4
$NiCr_{1.0}Fe_{1.0}O_4$	0.45	0.69	0.43	1.23	39.2	0.40	466	0.37	447	0.30	20.8
$NiCr_{1.2}Fe_{0.8}O_4$	0.43	0.74	0.42	1.28	37.9	0.39	454	0.39	435	0.29	23.8

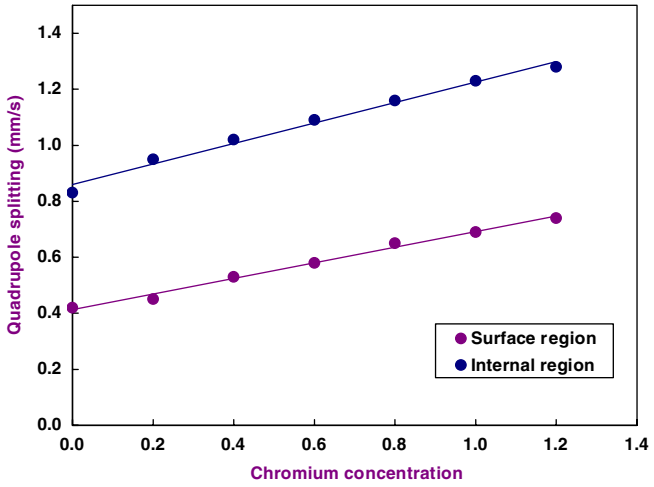

Fig. 6. Variation of quadrupole splitting with chromium concentration.

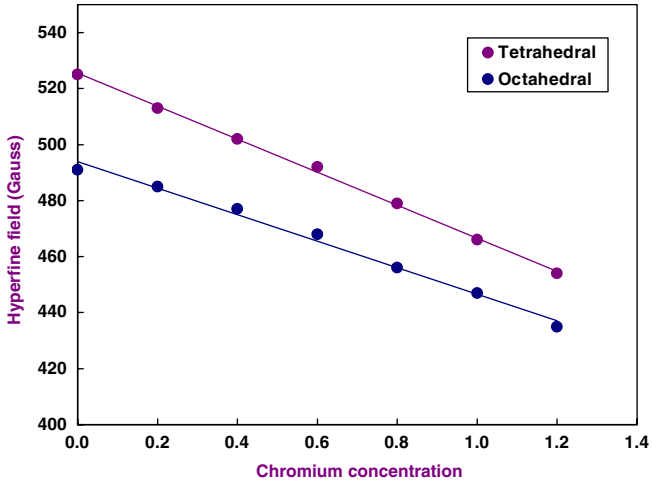

Fig. 7. Variation of hyperfine field with chromium concentration.

that there is a monotonic decrease in the internal hyperfine field values with increasing chromium substitution. This happens, because the replacement of Fe^{3+} by Cr^{3+} influences the internal hyperfine field of the nearest Fe^{3+} sites through super transferred hyperfine fields [27]. The cation distribution estimated using the intensity ratio of tetrahedral and octahedral sites is given in Table 2. The data indicates that the intensity of octahedral site decreases up to $x = 0.8$, after which it starts increasing. This increase is in conformity with the coercivity behaviour of the sample as discusses earlier. The cation distribution estimated using XRD, magnetic and Mössbauer measurements matches very well.

4. Conclusions

Cation distribution estimated from the XRD, magnetic and Mössbauer measurements indicates that the chromium atom occupy octahedral site upto $x = 0.8$, and then also enters into the tetrahedral site. The saturation magnetization decreases linearly with the increase of chromium concentration, however, coercivity increases slowly with the chromium concentration but when $x > 0.8$ a very large change has been observed. This was attributed to the cation distribution of Cr^{3+} due to an unquenched orbital angular momentum and a large anisotropy.

Acknowledgments

Thanks are due to the Department of Science and Technology, New Delhi, for providing the grant under fast track proposal for young scientist to S.S.

References

[1] J. Smit, H.P.J. Wijn, Ferrites, Philips Technical Library, 1959.
[2] K. Ishino, Y. Narumiya, Ceram. Bull. 66 (1987) 1469.
[3] P.I. Slick, in: E.P. Wohlfarth (Ed.), Ferromagnetic Materials, vol. 2, North-Holland, Amsterdam, 1980, p. 196.
[4] T. Abraham, Am. Ceram. Soc. Bull. 73 (1994) 62.
[5] D. Fiorani, in: J.L. Dormann, D. Fiorani (Eds.), Magnetic Properties of Fine Particles, Elsevier, North-Holland Delta Series, London, 1992.
[6] D.K. Kim, Y. Zhang, W. Voit, K.V. Rao, M. Muhammed, J. Magn. Magn. Mater. 225 (2001) 30.
[7] S.H. Lee, S.J. Yoon, G.J. Lee, H.S. Kim, C.H. Yo, K. Ahn, D.H. Lee, K.H. Kim, Mater. Chem. Phys. 61 (1999) 147.
[8] M.K. Fayek, S.S. Ata Allah, Phys. Stat. Sol. (a) 198 (2003) 457.
[9] A.M. Gismelseed, A.A. Yousif, Physica B 370 (2005) 215.
[10] A.K. Ghatage, S.A. Patil, S.K. Paranjpe, Solid State Commun. 98 (1996) 885.
[11] N.S. Satya Murthy, M.G. Matera, S.I. Youssef, R.J. Begum, Phys. Rev. 181 (1969) 969.
[12] E.J.E.J. Cukauskas, L.H. Allen, H.S. Newman, R.L. Henry, P.K. Van Damme, J. Appl. Phys. 67 (1990) 6946.
[13] M.J. Hampden-Smith, T.T. Kodas, J. Aerosol Sci. 26 (1995) S547.
[14] S. Singhal, A.N. Garg, K. Chandra, J. Magn. Magn. Mater. 285 (2005) 193.
[15] S. Singhal, S.K. Barthwal, K. Chandra, J. Solid. State. Chem. 178 (2005) 3183.
[16] J.E. Burke, Trans. Metall. Soc. AIME 180 (1949) 73.
[17] J.E. Burke, D. Tunbull, Prog. Met. Phys. 3 (1952) 220.
[18] H.P. Klug, L.E. Alexander, X-ray Diffraction Procedures for Poly Crystalline and Amorphous Materials, second ed, Wiley, New York, 1974 (Chapetr 9).
[19] J.A. Toledo, M.A. Valenzuela, P. Bosch, H. Armendariz, A. Montoya, N. Nava, A. Vazquez, Appl. Catal. A 198 (2000) 215.
[20] M.G. Buerger, Crystal Structure Analysis, Wiley Interscience, New York, 1960.
[21] H. Ohnishi, T. Teranishi, J. Phys. Soc. Jpn. 6 (1969) 36.
[22] J.B. Good enough, A.L. Loeb, Phys. Rev. 9 (1953) 391.
[23] S.K. Banerjee, W. O'Reilly, IEEE Trans. Magnets 3 (1966) 463.
[24] L. Neel, C.R. Acad. Sci. 230 (1950) 375.
[25] Y.G. Ma, M.Z. Jin, M.L. Liu, G. Chen, Y. Sui, Y. Tian, G.J. Zhang, Y.Q. Jia, Mater. Chem. Phys. 65 (2000) 79.
[26] J.Y. Ying, G.H. Wang, H. Fuchs, R. Laschinsk, H. Gleiter, Mater. Lett. 15 (1992) 180.
[27] J.A. Dumesic, H. Topsoe, Adv. Catal. 27 (1977) 121.